www.acsnano.org

Adsorption-Controlled Growth and Magnetism in Epitaxial SrRuO₃ Films

Anusha Kamath Manjeshwar,* Sreejith Nair, Anil Kumar Rajapitamahuni, Richard D. James, and Bharat Jalan*



Downloaded via UNIV OF MINNESOTA on May 13, 2024 at 19:12:29 (UTC). See https://pubs.acs.org/sharingguidelines for options on how to legitimately share published articles.

Cite This: ACS Nano 2023, 17, 20999-21005



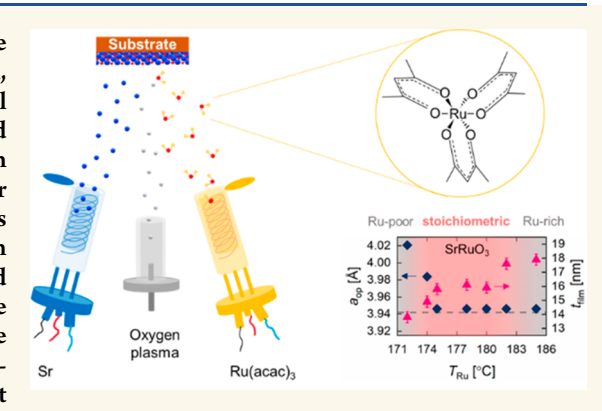
ACCESS I

III Metrics & More

Article Recommendations

Supporting Information

ABSTRACT: Controlling defect densities in SrRuO₃ films is the cornerstone for probing the intricate relationship among its structural, electrical, and magnetic properties. We combine film growth, electrical transport, and magnetometry to demonstrate the adsorption-controlled growth of phase-pure, epitaxial, and stoichiometric SrRuO₃ films on SrTiO₃ (001) substrates using solid source metal—organic molecular beam epitaxy. Across the growth window, we show that the anomalous Hall curves arise from two distinct magnetic domains. Domains with similar anomalous Hall polarities generate the stepped feature observed within the growth window, and those with opposite polarities produce the hump-like feature present exclusively in the highly Ru-poor film. We achieve a residual resistivity ratio (RRR = $\rho_{300\text{K}}/\rho_{2\text{K}}$) of 87 in a 50 nm-thick, coherently strained, and stoichometric SrRuO₃ film, the highest reported value to date on SrTiO₃ (001) substrates. We hypothesize



further improvements in the RRR through strain engineering to control the tetragonal-to-orthorhombic phase transformation and the domain structure of SrRuO₃ films.

KEYWORDS: adsorption-controlled growth, cation stoichiometry, metal—organic molecular beam epitaxy, magnetic domains, coercivity

1. INTRODUCTION

A metallic, 4d itinerant ferromagnetic perovskite oxide, SrRuO₃, has been widely studied for its rich intrinsic physics. SrRuO₃ is also a building block for the layered Sr_{n+1}Ru_nO_{3n+1}Ruddlesden—Popper materials, where *n* is the number of SrRuO₃ perovskite oxide layers sandwiched between two consecutive SrO rock salt layers. The observation and investigation of defect-sensitive properties in these materials such as the signatures of Weyl fermions in SrRuO₃, the unconventional superconductivity in Sr₂RuO₄, the electronic nematic order, and the quantum criticality in Sr₃Ru₂O₇ underscore the need for a high degree of control over the isolation of the desired layered phase and lowering its defect density.

Besides the discovery of new phenomena, SrRuO₃ films with controlled defect densities can potentially resolve long-standing debates on the origins of previously observed phenomena such as the hump-like features in their anomalous Hall curves.⁶ Some studies argue that the hump-like features arise from the topological Hall effect,⁷⁻¹¹ a manifestation of the enhanced Hall signal produced when the conduction electrons in SrRuO₃ interact with the skyrmion-produced magnetic field. Other studies contest this argument, suggesting that these features are associated with multiple magnetic

domains that arise from inhomogeneities in film thickness, Ru deficiency, the presence of different structural domains, or the stabilization of multiple crystal polymorphs of SrRuO₃. ^{12–20} Additional factors such as epitaxial strain-induced changes to the Berry phase curvature²¹ and proton intercalation into the SrRuO₃ lattice through ionic gating²² can produce changes in the anomalous Hall resistance and complicate this analysis. These observations highlight the intimate relationship among the structural, electrical, and magnetic properties of SrRuO₃. However, careful comparisons that account for the differences in thicknesses, stoichiometry, and growth conditions under which the hump-like features are observed are largely missing.

While the low energy of deposition in molecular beam epitaxy (MBE) is attractive for defect control in SrRuO₃, it has been challenging for three reasons: (1) the low vapor pressure of ruthenium (Ru), (2) its high electronegativity, and (3) the

Received: April 22, 2023
Accepted: September 12, 2023
Published: September 14, 2023





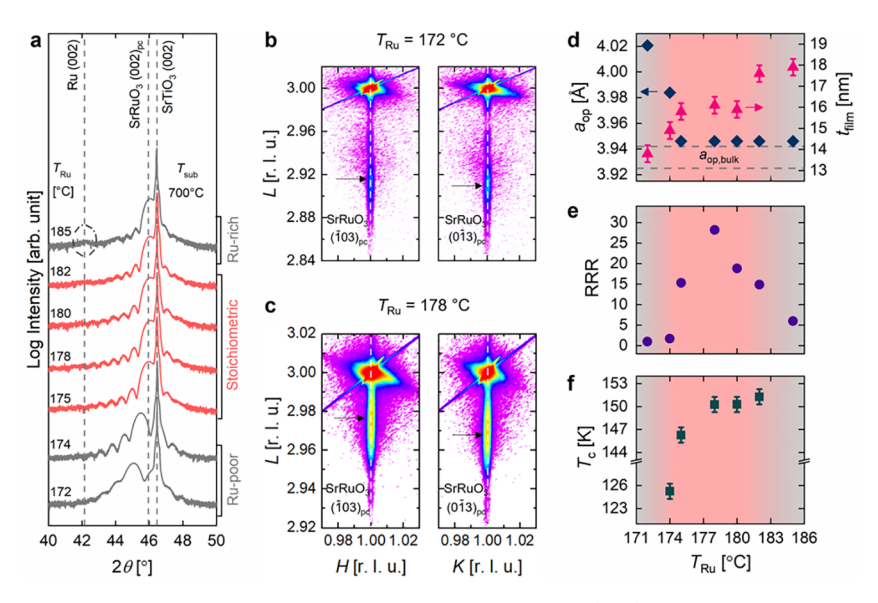


Figure 1. Adsorption-controlled growth window for $SrRuO_3$ films grown on $SrTiO_3$ (001) substrates at $T_{sub} = 700$ °C. (a) $2\theta - \omega$ coupled XRD scans showing the transition of film composition using different T_{Ru} across an adsorption-controlled growth window (plotted in red). A Ru (002) peak (circled) in the film grown at $T_{Ru} = 185$ °C indicates the film is Ru-rich. Reciprocal space maps about the $SrRuO_3$ ($\overline{103}$)_{pc} and ($\overline{013}$)_{pc} peaks for the films grown with a T_{Ru} of (b) 172 °C and (c) 178 °C show the coherence of the film to the substrate along the vertical dashed lines. The arrows show different peak positions in the out-of-plane direction, indicating orthorhombic crystal symmetry. (d) Evolution of the out-of-plane lattice parameter (a_{op} , left) and film thickness (t_{film} , right), (e) residual resistivity ratio (RRR), and (f) Curie temperature (T_c) across the growth window (shaded in red).

loss of supplied Ru as volatile oxides.²³ These challenges have been partially solved using electron beams to evaporate Ru, potent oxidants such as ozone to achieve the desired 4+ oxidation state, and by supplying an excess of Ru to counter its loss, respectively. We note that ozone and electron-beam assisted MBE succeeds at controlling the defect density of SrRuO₃ films by opening an adsorption-controlled growth window calculated by Nair et al.²³ Within these conditions conducive for phase-pure SrRuO3, any excess Ru is oxidized to its volatile oxides, which desorb from the growth front and are exhausted from the growth chamber. While these strategies have helped MBE achieve the lowest defect densities^{2,12,23-28} among all physical vapor deposition methods, 10,29-33 their implementation is expensive and requires intricate feedback loops to conform to the tight limits on stoichiometry and to ensure safe operation.

In this article, we demonstrate the adsorption-controlled growth of SrRuO₃ films using the sublimation of a solid metal organic precursor, Ru(acac)3, in a technique called solid source metal-organic molecular beam epitaxy (SSMOMBE) described elsewhere. 34,35 The metal-organic precursor contains pre-oxidized Ru and can be sublimed at T < 200 °C in an effusion cell as opposed to ~2000 °C required to evaporate the elemental Ru source in electron-beam assisted MBE. By harnessing the property of adsorption-controlled growth and carefully controlling the growth parameters in SSMOMBE, we interpret the origins of the changes in the anomalous Hall resistance as a function of cation stoichiometry and film thickness. We hypothesize an intricate relationship between the coercivities of the magnetic domains and the residual resistivity ratios (RRR) en route to controlling defect densities in SrRuO₃.

2. RESULTS AND DISCUSSIONS

2.1. Adsorption-Controlled Growth Window in Solid Source Metal—Organic MBE. We chose a substrate temperature $(T_{\rm sub})$ of 700 °C for the growth of SrRuO₃ films on SrTiO₃ (001) substrates since the density of Ru vacancies is known to increase at growth temperatures higher than 700 °C. ²³ We evaporated strontium (Sr) at a fixed beam equivalent pressure (BEP) of 3×10^{-8} Torr and sequentially increased the flux of Ru(acac)₃ by increasing the source temperature indicated by its thermocouple reading $(T_{\rm Ru})$. An inductively coupled radio frequency oxygen plasma source operated at a background pressure of 8×10^{-6} Torr and power of 300 W supplemented the oxygen in the Ru(acac)₃ during film growth.

The 2θ - ω coupled X-ray diffraction (XRD) scans in Figure 1a reveal two changes with increasing T_{Ru} : (1) a shift in the position of the SrRuO₃ (002)_{pc} peak (subscript "pc" indicates pseudocubic) and (2) the appearance of a peak from the Ru metal. Using a Poisson ratio ν = 0.3 for a typical perovskite oxide, 36 we expect an out-of-plane lattice parameter (a_{op}) of 3.942 Å for the low-temperature orthorhombic,³⁷ 3.987 Å for the intermediate-temperature tetragonal, 38 and 3.999 Å for the high-temperature cubic polymorphs³⁸ of SrRuO₃ strained coherently to the SrTiO₃ (001) substrate. With increasing $T_{\rm Ru}$ from 172 to 174 °C, the films showed a decrease in $a_{\rm op}$ from 4.021 ± 0.002 Å to 3.984 ± 0.002 Å. The film grown with $T_{\rm Ru}$ = 172 °C remained coherently strained to the substrate, as shown in the reciprocal space maps (Figure 1b), so we expect the higher a_{op} in this range to be a consequence of the higher density of Ru vacancies under growth conditions with intentionally low Ru(acac)₃ fluxes. The upshift of the $(\overline{103})_{pc}$ film peak compared to its $(0\overline{1}3)_{pc}$ peak along the out-of-plane (L) direction suggests the stabilization of the orthorhombic phase of SrRuO₃ on SrTiO₃ (001).¹⁸ Within this range of fluxes and for a fixed growth time, increasing T_{Ru} also resulted

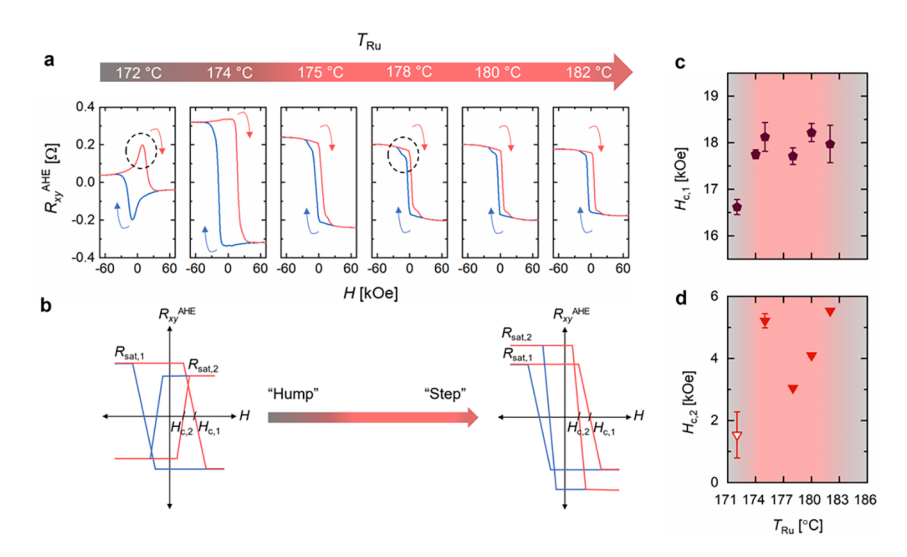


Figure 2. Evolution of anomalous Hall resistance as a function of $T_{\rm Ru}$. (a) Anomalous Hall resistance ($R_{xy}^{\rm AHE}$) of SrRuO₃ films grown with 172 °C $\leq T_{\rm Ru} \leq$ 182 °C measured at 50 K. The magnetic field is applied along the out-of-plane direction, i.e., $B \parallel [001]_{\rm sub}$. The blue curve indicates the Hall resistance measured during the magnetic field sweep from 90 to -90 kOe, and the red curve indicates the Hall resistance from the magnetic field sweep from -90 to 90 kOe. $R_{xy}^{\rm AHE}$ is plotted between -70 and 70 kOe so that the hump-like features (circled for $T_{\rm Ru}$ = 172 °C) and stepped features (circled for $T_{\rm Ru}$ = 178 °C) are visible. (b) Schematic of the superposition of the anomalous Hall curves of magnetic domains of opposite polarity producing the hump-like feature and magnetic domains of similar polarity producing the stepped feature (circled in (a)). Coercivities (c) $H_{\rm c,1}$ and (d) $H_{\rm c,2}$ as a function of $T_{\rm Ru}$. The solid symbols in (c) and (d) indicate the negative polarity of the anomalous Hall curve, and the hollow symbols indicate its positive polarity.

in an increase in film thickness (t_{film}) , shown in Figure 1d, which signifies a Ru flux-limited growth regime. When 175 ≤ $T_{\rm Ru} \leq 182$ °C, the films showed only the SrRuO₃ (00L)_{pc} peaks with a constant a_{op} of 3.946 \pm 0.002 Å, corresponding to the coherently strained, stoichiometric, orthorhombic phase. The predicted strain state and polymorph were seconded by the reciprocal space maps shown for a representative film (grown at $T_{Ru} = 178$ °C) within this range of fluxes (Figure 1c). Furthermore, within this range, t_{film} remained unchanged, suggesting an adsorption-controlled growth window (shaded in red) where the films self-regulate their stoichiometry by desorbing excess Ru-containing species from the growth front. At T_{Ru} = 185 °C, we observed a Ru (002) peak (circled in Figure 1a) in addition to the $(00L)_{pc}$ peaks of SrRuO₃, which implies that the growth is no longer adsorption-controlled. Consistent with our expectations, the RRRs of the stoichiometric and phase-pure SrRuO₃ films were higher than the RRRs of the films outside the growth window. However, the RRRs also varied within the growth window, increasing from \sim 15 at both boundaries to \sim 28 at the center of the growth window (Figure 1e), despite no indications of structural differences within the resolution of X-ray diffraction. The surface morphology of the films observed with atomic force microscopy (AFM) does not correlate with the stoichiometry and cannot explain the trend in RRR (Figure S1, Supporting Information). These observations raise two questions: (1) Does the change in RRR imply that stoichiometry varies within the "growth window"? (2) Could the change in RRR within the "growth window" be a consequence of subtle structural changes due to different growth conditions rather than differences in stoichiometry?

To address these questions, we examined the magnetic properties, such as the Curie temperature for the paramagnetic-to-ferromagnetic phase transformation (T_c) and the coercivity of magnetic domains in SrRuO₃ films within and outside the growth window. We exclude the Ru-rich films from

our comparison to eliminate contributions from elemental ruthenium. In Figure 1f, T_c , determined from the slope of temperature-dependent resistivity $(d\rho/dT)$, is plotted for various $T_{\rm Ru}^{39,40}$ The $T_{\rm c} \sim 150$ K remained nominally unchanged for films grown with 175 $^{\circ}$ C < $T_{\rm Ru} \leq$ 182 $^{\circ}$ C within the growth window and is comparable to the T_c of compressively strained SrRuO3 films grown by other techniques. 2,23,25,41 We observed a slight decrease in T_c toward the Ru-deficient boundary ($T_c = 147 \text{ K}$ at $T_{Ru} = 175 ^{\circ}\text{C}$), followed by a significant drop for Ru-deficient films ($T_c = 125$ K at $T_{\rm Ru}$ = 174 °C). The film grown at $T_{\rm Ru}$ = 172 °C did not show a clear divergence in $d\rho/dT$, making it difficult to determine T_c by this method, and is therefore excluded from the plot. This film, however, showed a hysteretic anomalous Hall resistance (discussed below) for $T \leq 125$ K, which suggests magnetic ordering in this temperature range.

In Figure 2a, we examined the anomalous Hall resistance of the films at 50 K since the field cooled M-T curve shows that the magnetization is saturated at this temperature even when films are Ru-poor (Figure S2, Supporting Information). At 50 K, we only observed a hump-like feature (circled in Figure 2a) in the anomalous Hall curve of the highly Ru-poor film grown with T_{Ru} = 172 °C. In contrast, all the films within the growth window showed a stepped feature (circled in Figure 2a for $T_{\rm Ru}$ = 178 °C). Within a two-domain picture, reports ^{12,13,15–20} interpret both the hump-like feature and the stepped feature in the observed anomalous Hall curves as an outcome of the superposition of the anomalous Hall curves from two magnetic domains of coercivities $H_{c,1}$ and $H_{c,2}$ (< $H_{c,1}$), illustrated schematically in Figure 2b. We extract the coercivities $H_{c,1}$ and $H_{c,2}$ from the peaks in the field derivative of the anomalous Hall resistance $(dR_{xy}^{AHE}/dH)^{18}$ (Figure S3, Supporting Information). The domain with the coercivity $H_{c,1}$ (filled pentagon) showed a negative anomalous Hall polarity (i.e., anomalous Hall behavior with negative saturated anomalous Hall resistance at a positive magnetic field) irrespective of

stoichiometry. The domain with the coercivity $H_{\rm c,2}$ (triangle symbol) had a negative polarity (filled inverted triangle) within the growth window, and its superposition on the domain with coercivity $H_{\rm c,1}$ reconstructed the stepped feature. We could only extract a single coercivity of the order of magnitude of $H_{\rm c,1}$ of the stoichiometric films within the margin of error of the peak fit for a slightly Ru-poor film grown with $T_{\rm Ru}=174$ °C. On increasing Ru deficiency further, the polarity of the domain with coercivity $H_{\rm c,2}$ selectively changed from negative to positive (open inverted triangle), generating the hump-like feature in the resultant anomalous Hall curve.

In addition to the qualitative differences in the polarities of the magnetic domains as a function of $T_{\rm Ru}$, we quantified the differences in the coercivities of the domains. While $H_{\rm c,1}$ varies by 3% within the growth window (Figure 2c), $H_{\rm c,2}$ decreases by ~40% from both boundaries of the growth window to the center (Figure 2d). Notably, a decrease in $H_{\rm c,2}$ coincides with an increase in RRR (Figure 1e), implying that the easier switching of the magnetization of this domain may be associated with a higher RRR. Since magnetization is sensitive to the structure, our hypothesis that there may be subtle structural changes in the films within the growth window from the distribution of pinning centers for magnetization switching (such as inhomogeneities at the nanoscale) due to the different growth conditions and kinetics 12,42 that are not captured by laboratory-based X-ray diffraction appears plausible.

2.2. Thickness Dependence of the Structural and Magnetic Properties of SrRuO₃ Films. To decouple the effect of stoichiometry from our study of coercivities and RRR, we grew films of different thicknesses (4 nm $\leq t_{\text{film}} \leq 50 \text{ nm}$) at a fixed stoichiometry within an adsorption-controlled growth window at T_{sub} = 800 °C. We chose film thicknesses such that the films remained coherently strained to the substrate (a reciprocal space map of the 50 nm-thick film in the inset of Figure 3a shows similar in-plane lattice parameters of the substrate and the film for the $(103)_{pc}$ peak) to avoid misfit dislocation-driven structural relaxation, which complicates the interpretation of the structure and its effect on the magnetic properties. The normalized resistivity (ρ/ρ_{2K}) of the stoichiometric SrRuO₃ films at 4 nm $\leq t_{\text{film}} \leq$ 50 nm shows a transition from semiconducting-like behavior for film with $t_{\text{film}} = 4 \text{ nm}$ to metallic behavior for thicker films (Figure 3a). The T_c increased monotonically from 147 K for the 8 nm-thick film to 151 K for the 50 nm-thick film. Though the T_c for the 4 nm-thick film was indistinguishable from the divergence of $d\rho$ dT, it showed an anomalous Hall resistance at $T \le 125$ K, which is symbolic of its magnetic behavior at these temperatures.

With increasing film thickness, the $a_{\rm op}$ of SrRuO₃ decreased from ~3.98 Å for the 4 nm-thick film to $(3.942-3.949) \pm 0.002$ Å for films with 8 nm $\leq t_{\rm film} \leq 50$ nm (Figure 3b). The higher $a_{\rm op}$ in the 4 nm film suggests the presence of a fully strained tetragonal polymorph of SrRuO₃ from the suppressed in-plane octahedral rotations due to its proximity with the cubic SrTiO₃ (001) substrate. In fact, the stabilization of the tetragonal polymorph of SrRuO₃ has been reported in up to 18 unit cell-thick SrRuO₃ films on SrTiO₃ (001). The lower $a_{\rm op}$ for the thicker films is in agreement with the stabilization of the fully coherent orthorhombic polymorph of SrRuO₃.

We plot $H_{c,1}$ and $H_{c,2}$ as a function of $t_{\rm film}$ (Figure 3c) and find that the coercivities of both domains decreased with increasing $t_{\rm film}$. We were only able to extract one coercivity within the margin of error of the peak fit of $dR_{xy}^{\rm AHE}/dH$ for the

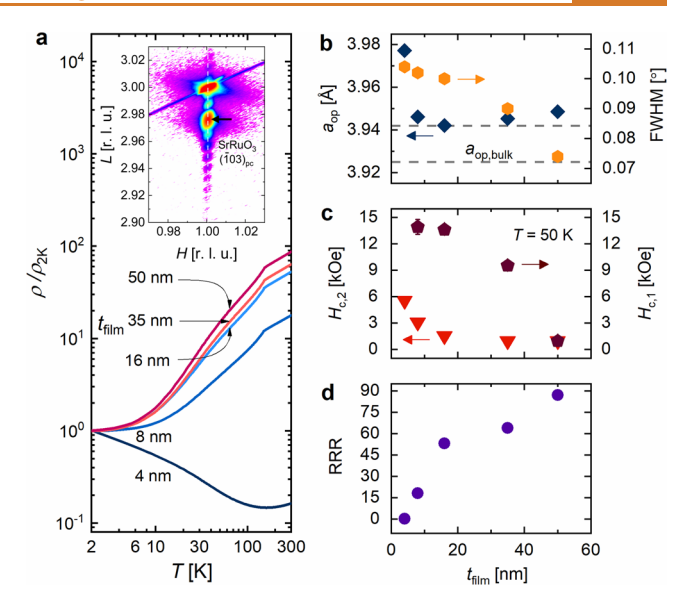


Figure 3. Effect of the thickness of SrRuO₃ films grown under identical conditions within an adsorption-controlled growth window on its structural, electrical, and magnetic properties. (a) Temperature-dependent resistivities of $t_{\rm film}$ -thick SrRuO₃ films on SrTiO₃ (001) substrates normalized by their corresponding resistivities at 2 K. (inset) Reciprocal space map about the $(\bar{1}03)_{\rm pc}$ peak of the 50 nm-thick SrRuO₃ film shows it is coherent with the SrTiO₃ (001) substrate. Thickness dependence of (b) the out-of-plane lattice parameter ($a_{\rm op}$, left) and the full width at half-maximum (FWHM) of the rocking curve about the SrRuO₃ (002)_{pc} peak (right), (c) the coercivities of the two magnetic domains $H_{\rm c,1}$ (right) and $H_{\rm c,2}$ (left), and (d) residual resistivity ratio (RRR).

4 nm-thick film (Figure S4, Supporting Information) and hypothesize that it is associated with the tetragonal polymorph which we expect from $a_{\rm op}$. Similarly, at $t_{\rm film}$ = 50 nm, we could again only extract one coercivity which we assign to the orthorhombic polymorph in accordance with a_{op} . At intermediate thicknesses, the coercivities of the two domains were sufficiently resolved and could be extracted from the peaks in the field derivative of the anomalous Hall resistance (Figure S4). We hypothesize that the two domains arise from the presence of mixed phases at intermediate thicknesses in the structural phase transformation, similar to the structural phase transformation in fully coherent films of SrSnO₃.⁴⁴ These results are in agreement with the recent synchrotron X-raybased study, which revealed subtle structural changes in SrRuO₃ films as a function of film thickness despite being fully commensurate with the substrate.⁴⁵

Consistent with our observation in Figure 2d, the decrease in $H_{\rm c,2}$ again coincides with the increase in the RRR (Figure 3d). Taken together with the decrease in the full width at half-maximum (FWHM) of the rocking curve about the SrRuO₃ (002)_{pc} peak with increasing film thickness (Figure 3b), the decrease in $H_{\rm c,2}$ under fixed growth conditions points to a decrease in the fraction of the domains associated with the tetragonal polymorph and its boundaries with the other. Since the stoichiometry was kept fixed, these observations underscore that the observed change in coercivities and RRR is related to structural changes from the thickness-dependent tetragonal-to-orthorhombic phase transformation and not the stoichiometry. Future theoretical investigations combined with magnetic domain imaging and transmission electron micros-

copy should be directed to understand the origins of these domains, their distribution, and the microscopic correlation between domain structure, coercivities, and RRR in SrRuO₃.

2.3. Feasibility of SSMOMBE for Defect-Controlled Growth of SrRuO₃. We now compare the RRR of SrRuO₃ films across different synthesis approaches, epitaxial strains, and film thicknesses in Figure 4. Films grown by electron-beam

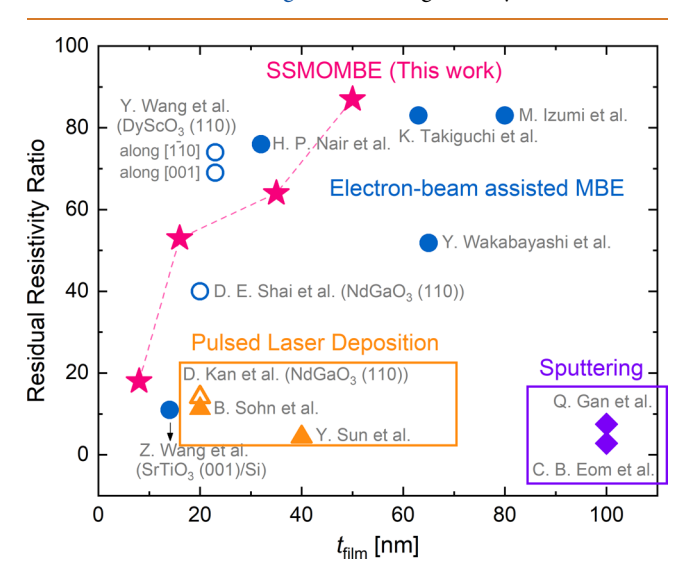


Figure 4. Residual resistivity ratio (RRR) of SrRuO₃ as a function of film thickness ($t_{\rm film}$) for different synthesis approaches and substrates. Films grown by solid source metal—organic molecular beam epitaxy (SSMOMBE) are indicated by star symbols, electron-beam assisted molecular beam epitaxy (MBE) by circles, $^{2,23-28}$ pulsed laser deposition (PLD) by triangles, 10,31,33 and sputtering by diamond symbols. 29,30 The filled symbols indicate that the SrRuO₃ films are grown on SrTiO₃ (001) substrates. The substrates for the films indicated by the hollow symbols are written next to the authors of the corresponding report. The RRR of 130 reported for a SrRuO₃ film on a DyScO₃ (110) substrate is not plotted due to its missing film thickness in the report. 12

assisted MBE (circle symbol) usually have higher RRRs across all the above parameters compared to films grown by pulsed laser deposition (triangle symbol) and sputtering (diamond symbol). Guided by an adsorption-controlled growth window in SSMOMBE, we achieve comparable or even higher RRRs in SrRuO₃ films on SrTiO₃ (001) substrates (stars with dashed lines) than those of electron-beam assisted MBE-grown films on these substrates (filled circles). The RRR of 87 in the 50 nm-thick, coherently strained film grown by SSMOMBE exceeds previously reported values of RRR in SrRuO3 films on SrTiO₃ (001) substrates across all film thicknesses and synthesis techniques. These observations reveal that the adsorption-controlled growth window, coupled with the understanding of growth parameters and structure we developed in this paper, presents a simple route to SrRuO3 films with improved defect densities.

3. CONCLUSIONS

We demonstrate the adsorption-controlled growth of phasepure, epitaxial $SrRuO_3$ thin films on $SrTiO_3$ (001) substrates using solid source metal—organic MBE. At 50 K, we observe a hump-like feature only in the anomalous Hall resistance of the highly Ru-deficient film and a stepped feature in all stoichiometric films. We argue that both of these features arise from the superposition of the contributions to the anomalous Hall resistance from two distinct magnetic domains. Within the growth window, we noted that the coercivity of one of the two magnetic domains selectively decreases, accompanied by an increase in RRR. We attribute this change in magnetic domain structure and, consequently, the coercivities of the domains to the potentially different distribution of inhomogeneities at the nanoscale from different growth kinetics. By examining stoichiometric SrRuO3 films of different thicknesses grown under the same conditions, we reveal that the origin of the two domains and the changes in the coercivities and RRR with thickness are associated with subtle changes in the structure related to the tetragonal-toorthorhombic phase transformation. Using coercivity as a guideline for stoichiometry optimization, we achieve the highest of any previously reported RRR of a SrRuO3 film on SrTiO₃ (001) substrates (RRR = 87 for a 50 nm thick SrRuO₃ film). Our studies establish the important relationship between the magnetic domain structure and the RRR in SrRuO₃ films, guiding pathways to achieve higher RRR through domain and strain engineering.

4. EXPERIMENTAL METHODS

4.1. Film Growth. The SrRuO₃ thin films were grown on SrTiO₃ (001) substrates (Shinkosha Co., Japan, and Crystec GmbH, Germany) in an EVO 50 MBE system (Scienta Omicron, Germany) using solid source metal-organic molecular beam epitaxy described elsewhere. 34 The substrates were heated to temperatures (T_{sub}) of \sim 700–800 °C and cleaned for 20 min before the start of film growth with an inductively coupled radio-frequency oxygen plasma (Mantis, UK) operated at 300 W and at an oxygen pressure of \sim 8 × 10⁻⁶ Torr. Strontium (99.99%, Sigma-Aldrich, USA) was evaporated from an effusion cell (MBE Komponenten, Germany) at a BEP of 3×10^{-8} Torr. Ruthenium was supplied by subliming a solid metal-organic precursor, Ru(acac)₃ (99.99%, American Elements, USA), from an effusion cell at thermocouple temperature readings (T_{Ru}) of 172–185 °C. An inductively coupled radio-frequency oxygen plasma (Mantis, UK) operated at 300 W and at an oxygen pressure of \sim 8 × 10⁻⁶ Torr was used during the growth of all films. The films in the thickness series were grown at $T_{\rm sub}$ = 800 °C with $T_{\rm Ru}$ = 184 °C, ensuring that the films were within an adsorption-controlled growth window.

4.2. Structural Characterization. The composition of the films and their epitaxial relationship with the substrate were determined using high-resolution X-ray diffraction (HRXRD) in a SmartLab XE diffractometer (Rigaku, USA) with a Ge (220) monochromator. The thickness of the films ($t_{\rm film}$) was extracted by fitting the oscillations in the grazing incidence X-ray reflectometry (GIXR) measurements. The surface morphology of the films was measured on a Nanoscope V Multimode 8 atomic force microscope (Bruker, USA).

4.3. Characterization of Electrical and Magnetic Properties. The longitudinal and Hall four-terminal resistances were measured in a DynaCool Physical Property Measurement System (PPMS, Quantum Design, USA). Aluminum wire bonding was used to make Ohmic contacts in the Van der Pauw geometry. ⁴⁶ The Curie temperature was extracted from the temperature at which the slope of the temperature-dependent resistivity diverges. RRR was calculated from the ratio of the resistivities at 300 and 2 K.

All Hall resistances were antisymmetrized. The linear ordinary Hall component obtained from the slope of the Hall resistance at high magnetic fields (typically > 30 kOe at 50 K) was subtracted from the antisymmetrized Hall resistance to yield the anomalous Hall resistance.

Field cooled M-T curves were measured between 10 and 250 K using the Vibrating Sample Magnetometer (VSM) module in an EverCool PPMS (Quantum Design, USA). The films were mounted on a quartz paddle with the magnetic field parallel to the [100]_{sub} direction. They were first cooled in a magnetic field of 70 kOe, and

the magnetization was recorded while heating using a sense field of 1000 Oe after stabilizing the temperature at intervals of 5 K.

ASSOCIATED CONTENT

Data Availability Statement

All data needed to evaluate the conclusions of the paper are present in the paper and/or the Supporting Information.

Supporting Information

The Supporting Information is available free of charge at https://pubs.acs.org/doi/10.1021/acsnano.3c03625.

Details of the surface morphology of the $SrRuO_3$ films, the field-cooled temperature-dependent magnetization, and the extraction of the coercivities of the magnetic domains as a function of $Ru(acac)_3$ effusion cell temperature (T_{Ru}) and film thickness (t_{film}) (PDF)

AUTHOR INFORMATION

Corresponding Authors

Anusha Kamath Manjeshwar – Department of Chemical Engineering and Materials Science, University of Minnesota–Twin Cities, Minneapolis, Minnesota 55455, United States; Email: kamat086@umn.edu

Bharat Jalan — Department of Chemical Engineering and Materials Science, University of Minnesota—Twin Cities, Minneapolis, Minnesota 55455, United States; orcid.org/0000-0002-7940-0490; Email: bjalan@umn.edu

Authors

Sreejith Nair — Department of Chemical Engineering and Materials Science, University of Minnesota—Twin Cities, Minneapolis, Minnesota 55455, United States

Anil Kumar Rajapitamahuni – Department of Chemical Engineering and Materials Science, University of Minnesota–Twin Cities, Minneapolis, Minnesota 55455, United States

Richard D. James – Department of Aerospace Engineering and Mechanics, University of Minnesota–Twin Cities, Minneapolis, Minnesota 55455, United States

Complete contact information is available at: https://pubs.acs.org/10.1021/acsnano.3c03625

Author Contributions

A.K.M., A.K.R., R.D.J., and B.J. conceptualized and designed the experiments. A.K.M. and S.N. grew the thin films and characterized their structure using X-ray diffraction and atomic force microscopy. A.K.M. and A.K.R. performed the electrical transport measurements. A.K.M. performed the magnetometry measurements. A.K.M. and B.J. wrote the manuscript. All authors contributed to the discussion of the results and reviewed the manuscript. B.J. directed and organized different aspects of the project.

Notes

The authors declare no competing financial interest.

ACKNOWLEDGMENTS

Film growth and characterization (A.K.M. and B.J.) was supported by the U.S. Department of Energy through DE-SC0020211. S.N. acknowledges partial support from the Air Force Office of Scientific Research (AFOSR) through Grant Nos. FA9550-21-1-0025 and FA9550-21-0460. This work also benefitted from the Vannevar Bush Faculty Fellowship. S.N. and A.K.R. were supported partially by the UMN MRSEC

program under Award No. DMR-2011401. Parts of this work were carried out in the College of Science and Engineering Characterization Facility at the University of Minnesota, which receives partial support from the National Science Foundation through the Materials Research Science and Engineering Center (MRSEC, Award No. DMR-2011401) and the National Nanotechnology Coordinated Infrastructure (NNCI, Award No. ECCS-2025124) programs. A.K.M. also acknowledges the University of Minnesota Doctoral Dissertation Fellowship.

REFERENCES

- (1) Koster, G.; Klein, L.; Siemons, W.; Rijnders, G.; Dodge, J. S.; Eom, C.-B.; Blank, D. H. A.; Beasley, M. R. Structure, Physical Properties, and Applications of SrRuO₃ Thin Films. *Rev. Mod. Phys.* **2012**, *84* (1), 253–298.
- (2) Takiguchi, K.; Wakabayashi, Y. K.; Irie, H.; Krockenberger, Y.; Otsuka, T.; Sawada, H.; Nikolaev, S. A.; Das, H.; Tanaka, M.; Taniyasu, Y.; Yamamoto, H. Quantum Transport Evidence of Weyl Fermions in an Epitaxial Ferromagnetic Oxide. *Nat. Commun.* 2020, 11 (1), 4969.
- (3) Mackenzie, A. P.; Maeno, Y. The Superconductivity of Sr_2RuO_4 and the Physics of Spin-Triplet Pairing. *Rev. Mod. Phys.* **2003**, 75 (2), 657–712.
- (4) Borzi, R. A.; Grigera, S. A.; Farrell, J.; Perry, R. S.; Lister, S. J. S.; Lee, S. L.; Tennant, D. A.; Maeno, Y.; Mackenzie, A. P. Formation of a Nematic Fluid at High Fields in Sr₃Ru₂O₇. Science **2007**, 315 (5809), 214–217.
- (5) Stingl, C.; Perry, R. S.; Maeno, Y.; Gegenwart, P. Electronic Nematicity and Its Relation to Quantum Criticality in Sr₃Ru₂O₇ Studied by Thermal Expansion. *Phys. Status Solidi B* **2013**, 250 (3), 450–456.
- (6) Nagaosa, N.; Sinova, J.; Onoda, S.; MacDonald, A. H.; Ong, N. P. Anomalous Hall Effect. *Rev. Mod. Phys.* **2010**, 82 (2), 1539–1592. (7) Lu, J.; Si, L.; Zhang, Q.; Tian, C.; Liu, X.; Song, C.; Dong, S.; Wang, J.; Cheng, S.; Qu, L.; Zhang, K.; Shi, Y.; Huang, H.; Zhu, T.; Mi, W.; Zhong, Z.; Gu, L.; Held, K.; Wang, L.; Zhang, J. Defect-Engineered Dzyaloshinskii—Moriya Interaction and Electric-Field-Switchable Topological Spin Texture in SrRuO₃. *Adv. Mater.* **2021**, 33 (33), 2102525.
- (8) Wang, C.; Chang, C.; Herklotz, A.; Chen, C.; Ganss, F.; Kentsch, U.; Chen, D.; Gao, X.; Zeng, Y.; Hellwig, O.; Helm, M.; Gemming, S.; Chu, Y.; Zhou, S. Topological Hall Effect in Single Thick SrRuO₃ Layers Induced by Defect Engineering. *Adv. Electron. Mater.* **2020**, *6* (6), 2000184.
- (9) Qin, Q.; Liu, L.; Lin, W.; Shu, X.; Xie, Q.; Lim, Z.; Li, C.; He, S.; Chow, G. M.; Chen, J. Emergence of Topological Hall Effect in a SrRuO₃ Single Layer. *Adv. Mater.* **2019**, *31* (8), 1807008.
- (10) Sohn, B.; Kim, B.; Choi, J. W.; Chang, S. H.; Han, J. H.; Kim, C. Hump-like Structure in Hall Signal from Ultra-Thin SrRuO₃ Films without Inhomogeneous Anomalous Hall Effect. *Curr. Appl. Phys.* **2020**, *20* (1), 186–190.
- (11) Sohn, B.; Kim, B.; Park, S. Y.; Choi, H. Y.; Moon, J. Y.; Choi, T.; Choi, Y. J.; Zhou, H.; Choi, J. W.; Bombardi, A.; Porter, Dan. G.; Chang, S. H.; Han, J. H.; Kim, C. Stable Humplike Hall Effect and Noncoplanar Spin Textures in SrRuO₃ Ultrathin Films. *Phys. Rev. Research* 2021, 3 (2), No. 023232.
- (12) Kim, G.; Son, K.; Suyolcu, Y. E.; Miao, L.; Schreiber, N. J.; Nair, H. P.; Putzky, D.; Minola, M.; Christiani, G.; van Aken, P. A.; Shen, K. M.; Schlom, D. G.; Logvenov, G.; Keimer, B. Inhomogeneous Ferromagnetism Mimics Signatures of the Topological Hall Effect in SrRuO₃ Films. *Phys. Rev. Materials* **2020**, *4* (10), 104410
- (13) Kan, D.; Moriyama, T.; Kobayashi, K.; Shimakawa, Y. Alternative to the Topological Interpretation of the Transverse Resistivity Anomalies in SrRuO₃. Phys. Rev. B **2018**, 98 (18), 180408.

- (14) Kan, D.; Moriyama, T.; Shimakawa, Y. Field-Sweep-Rate and Time Dependence of Transverse Resistivity Anomalies in Ultrathin SrRuO₃ Films. *Phys. Rev. B* **2020**, *101* (1), No. 014448.
- (15) Gerber, A. Interpretation of Experimental Evidence of the Topological Hall Effect. *Phys. Rev. B* **2018**, 98 (21), 214440.
- (16) Wu, L.; Wen, F.; Fu, Y.; Wilson, J. H.; Liu, X.; Zhang, Y.; Vasiukov, D. M.; Kareev, M. S.; Pixley, J. H.; Chakhalian, J. Berry Phase Manipulation in Ultrathin SrRuO₃ Films. *Phys. Rev. B* **2020**, 102 (22), 220406.
- (17) Wang, L.; Feng, Q.; Lee, H. G.; Ko, E. K.; Lu, Q.; Noh, T. W. Controllable Thickness Inhomogeneity and Berry Curvature Engineering of Anomalous Hall Effect in SrRuO₃ Ultrathin Films. *Nano Lett.* **2020**, *20* (4), 2468–2477.
- (18) Wang, W.; Li, L.; Liu, J.; Chen, B.; Ji, Y.; Wang, J.; Cheng, G.; Lu, Y.; Rijnders, G.; Koster, G.; Wu, W.; Liao, Z. Magnetic Domain Engineering in SrRuO₃ Thin Films. *npj Quantum Mater.* **2020**, 5 (1), 73.
- (19) Han, H.; Zhou, H.; Guillemard, C.; Valvidares, M.; Sharma, A.; Li, Y.; Sharma, A. K.; Kostanovskiy, I.; Ernst, A.; Parkin, S. S. P. Reversal of Anomalous Hall Effect and Octahedral Tilting in SrRuO₃ Thin Films via Hydrogen Spillover. *Adv. Mater.* **2023**, 35 (3), 2207246.
- (20) Kimbell, G.; Sass, P. M.; Woltjes, B.; Ko, E. K.; Noh, T. W.; Wu, W.; Robinson, J. W. A. Two-Channel Anomalous Hall Effect in SrRuO₃. *Phys. Rev. Materials* **2020**, *4* (5), No. 054414.
- (21) Tian, D.; Liu, Z.; Shen, S.; Li, Z.; Zhou, Y.; Liu, H.; Chen, H.; Yu, P. Manipulating Berry Curvature of SrRuO₃ Thin Films via Epitaxial Strain. *Proc. Natl. Acad. Sci. U.S.A.* **2021**, *118* (18), No. e2101946118.
- (22) Li, Z.; Shen, S.; Tian, Z.; Hwangbo, K.; Wang, M.; Wang, Y.; Bartram, F. M.; He, L.; Lyu, Y.; Dong, Y.; Wan, G.; Li, H.; Lu, N.; Zang, J.; Zhou, H.; Arenholz, E.; He, Q.; Yang, L.; Luo, W.; Yu, P. Reversible Manipulation of the Magnetic State in SrRuO₃ through Electric-Field Controlled Proton Evolution. *Nat. Commun.* **2020**, *11* (1), 184.
- (23) Nair, H. P.; Liu, Y.; Ruf, J. P.; Schreiber, N. J.; Shang, S.-L.; Baek, D. J.; Goodge, B. H.; Kourkoutis, L. F.; Liu, Z.-K.; Shen, K. M.; Schlom, D. G. Synthesis Science of SrRuO₃ and CaRuO₃ Epitaxial Films with High Residual Resistivity Ratios. *APL Materials* **2018**, *6* (4), No. 046101.
- (24) Wang, Z.; Nair, H. P.; Correa, G. C.; Jeong, J.; Lee, K.; Kim, E. S.; H, A. S.; Lee, C. S.; Lim, H. J.; Muller, D. A.; Schlom, D. G. Epitaxial Integration and Properties of SrRuO₃ on Silicon. *APL Materials* **2018**, *6* (8), No. 086101.
- (25) Wakabayashi, Y. K.; Otsuka, T.; Krockenberger, Y.; Sawada, H.; Taniyasu, Y.; Yamamoto, H. Machine-Learning-Assisted Thin-Film Growth: Bayesian Optimization in Molecular Beam Epitaxy of SrRuO₃ Thin Films. *APL Materials* **2019**, *7* (10), 101114.
- (26) Izumi, M.; Nakazawa, K.; Bando, Y.; Yoneda, Y.; Terauchi, H. Magnetotransport of SrRuO $_3$ Thin Film on SrTiO $_3$ (001). *J. Phys. Soc. Jpn.* **1997**, 66 (12), 3893–3900.
- (27) Shai, D. E.; Adamo, C.; Shen, D. W.; Brooks, C. M.; Harter, J. W.; Monkman, E. J.; Burganov, B.; Schlom, D. G.; Shen, K. M. Quasiparticle Mass Enhancement and Temperature Dependence of the Electronic Structure of Ferromagnetic SrRuO₃ Thin Films. *Phys. Rev. Lett.* **2013**, *110* (8), No. 087004.
- (28) Wang, Y.; Bossé, G.; Nair, H. P.; Schreiber, N. J.; Ruf, J. P.; Cheng, B.; Adamo, C.; Shai, D. E.; Lubashevsky, Y.; Schlom, D. G.; Shen, K. M.; Armitage, N. P. Subterahertz Momentum Drag and Violation of Matthiessen's Rule in an Ultraclean Ferromagnetic SrRuO₃ Metallic Thin Film. *Phys. Rev. Lett.* **2020**, *125* (21), 217401.
- (29) Eom, C. B.; Cava, R. J.; Fleming, R. M.; Phillips, J. M.; vanDover, R. B.; Marshall, J. H.; Hsu, J. W. P.; Krajewski, J. J.; Peck, W. F. Single-Crystal Epitaxial Thin Films of the Isotropic Metallic Oxides $\mathrm{Sr}_{1-x}\mathrm{Ca}_x\mathrm{RuO}_3$ (0 \leq × \leq 1). Science 1992, 258 (5089), 1766–1769.
- (30) Gan, Q.; Rao, R. A.; Eom, C. B.; Garrett, J. L.; Lee, M. Direct Measurement of Strain Effects on Magnetic and Electrical Properties

- of Epitaxial SrRuO₃ Thin Films. Appl. Phys. Lett. 1998, 72 (8), 978–
- (31) Kan, D.; Aso, R.; Kurata, H.; Shimakawa, Y. Epitaxial Strain Effect in Tetragonal SrRuO₃ Thin Films. *J. Appl. Phys.* **2013**, *113* (17), 173912.
- (32) Kacedon, D. B.; Rao, R. A.; Eom, C. B. Magnetoresistance of Epitaxial Thin Films of Ferromagnetic Metallic Oxide SrRuO₃ with Different Domain Structures. *Appl. Phys. Lett.* **1997**, 71 (12), 1724–1726
- (33) Sun, Y.; Zhong, N.; Zhang, Y.-Y.; Qi, R.-J.; Huang, R.; Tang, X.-D.; Yang, P.-X.; Xiang, P.-H.; Duan, C.-G. Structure and Electrical Properties of Epitaxial SrRuO₃ Thin Films Controlled by Oxygen Partial Pressure. *J. Appl. Phys.* **2016**, *120* (23), 235108.
- (34) Nunn, W.; Manjeshwar, A. K.; Yue, J.; Rajapitamahuni, A.; Truttmann, T. K.; Jalan, B. Novel Synthesis Approach for "Stubborn" Metals and Metal Oxides. *Proc. Natl. Acad. Sci. U. S. A.* **2021**, *118* (32), No. e2105713118.
- (35) Nunn, W.; Nair, S.; Yun, H.; Kamath Manjeshwar, A.; Rajapitamahuni, A.; Lee, D.; Mkhoyan, K. A.; Jalan, B. Solid-Source Metal—Organic Molecular Beam Epitaxy of Epitaxial RuO₂. *APL Materials* **2021**, *9* (9), No. 091112.
- (36) Shin, J.; Kalinin, S. V.; Lee, H. N.; Christen, H. M.; Moore, R. G.; Plummer, E. W.; Baddorf, A. P. Surface Stability of Epitaxial SrRuO₃ Films. *Surf. Sci.* **2005**, *581* (2–3), 118–132.
- (37) Jones, C. W.; Battle, P. D.; Lightfoot, P.; Harrison, W. T. A. The Structure of SrRuO₃ by Time-of-Flight Neutron Powder Diffraction. *Acta Crystallogr. C Cryst. Struct Commun.* **1989**, 45 (3), 365–367.
- (38) Kennedy, B. J.; Hunter, B. A. High-Temperature Phases of SrRuO₃. *Phys. Rev. B* **1998**, *58* (2), *653*–*658*.
- (39) Chandra, P.; Littlewood, P. B. A Landau Primer for Ferroelectrics. In *Physics of Ferroelectrics: A Modern Perspective*; Springer Berlin Heidelberg: Berlin, Heidelberg, 2007; pp 69–116.
- (40) Spaldin, N. A. Interactions in Ferromagnetic Materials. In *Magnetic Materials: Fundamentals and Applications*; Cambridge University Press: Cambridge, 2010; pp 65–78.
- (41) Gao, R.; Dong, Y.; Xu, H.; Zhou, H.; Yuan, Y.; Gopalan, V.; Gao, C.; Fong, D. D.; Chen, Z.; Luo, Z.; Martin, L. W. Interfacial Octahedral Rotation Mismatch Control of the Symmetry and Properties of SrRuO₃. ACS Appl. Mater. Interfaces **2016**, 8 (23), 14871–14878.
- (42) Ko, E. K.; Lee, H. G.; Lee, S.; Mun, J.; Kim, J.; Lee, J. H.; Kim, T. H.; Chung, J.; Chung, S. B.; Park, S. H.; Yang, S. M.; Kim, M.; Chang, S. H.; Noh, T. W. Tunable Two-Channel Magnetotransport in SrRuO₃ Ultrathin Films Achieved by Controlling the Kinetics of Heterostructure Deposition. *Adv. Elect Materials* **2022**, 8 (2), 2100804.
- (43) Chang, S. H.; Chang, Y. J.; Jang, S. Y.; Jeong, D. W.; Jung, C. U.; Kim, Y.-J.; Chung, J.-S.; Noh, T. W. Thickness-Dependent Structural Phase Transition of Strained SrRuO₃ Ultrathin Films: The Role of Octahedral Tilt. *Phys. Rev. B* **2011**, *84* (10), 104101.
- (44) Truttmann, T. K.; Liu, F.; Garcia-Barriocanal, J.; James, R. D.; Jalan, B. Strain Relaxation via Phase Transformation in High-Mobility SrSnO₃ Films. *ACS Appl. Electron. Mater.* **2021**, *3* (3), 1127–1132.
- (45) Zhang, X.; Penn, A. N.; Wysocki, L.; Zhang, Z.; van Loosdrecht, P. H. M.; Kornblum, L.; LeBeau, J. M.; Lindfors-Vrejoiu, I.; Kumah, D. P. Thickness and Temperature Dependence of the Atomic-Scale Structure of SrRuO₃ Thin Films. *APL Materials* **2022**, *10* (5), No. 051107.
- (46) Van der Pauw, L. J. A Method of Measuring the Resistivity and Hall Coefficient on Lamellae of Arbitrary Shape. *Philips Technical Review* **1958**, *20*, 220–224.